ACS OMEGA

Open Access

http://pubs.acs.org/journal/acsodf

Article

Classical and Nonclassical Nucleation Mechanisms of Insulin Crystals

Joana Ferreira,* Vicente Domínguez-Arca, João Carneiro, Gerardo Prieto, Pablo Taboada, and João Moreira de Campos

Cite This: *ACS Omega* 2024, 9, 23364−23376

Read Online

ACCESS | Metrics & More | Article Recommendations | Supporting Information

ABSTRACT: Although the *Classical Nucleation Theory* (CNT) is the most consensual theory to explain protein nucleation mechanisms, experimental observations during the shear-induced assays suggest that the CNT does not always describe the insulin nucleation process. This is the case at intermediate precipitant ($ZnCl_2$) solution concentrations (2.3 mM) and high-temperature values (20 and 40 °C) as well as at low precipitant solution concentrations (1.6 mM) and low-temperature values (5 °C). In this work, crystallization events following the CNT registered at high precipitant solution concentrations (3.1 and 4.7 mM) are typically described by a Newtonian response. On the other hand, crystallization events following a nonclassical nucleation pathway seem to involve the formation of a metastable intermediate state before crystal formation and are described by a transition from Newtonian to shear-thinning responses. A dominant shear-thinning behavior (shear viscosity values ranging more than 6 orders of magnitude) is found during aggregation/agglomeration events. The rheological analysis is complemented with different characterization techniques (Dynamic Light Scattering, Energy-Dispersive Spectroscopy, Circular Dichroism, and Differential Scanning Calorimetry) to understand the insulin behavior in solution, especially during the occurrence of aggregation/agglomeration events. To the best of our knowledge, the current work is the first study describing nonclassical nucleation mechanisms during shear-induced crystallization experiments, which reveals the potential of the interdisciplinary approach herein described and opens a window for a clear understanding of protein nucleation mechanisms.

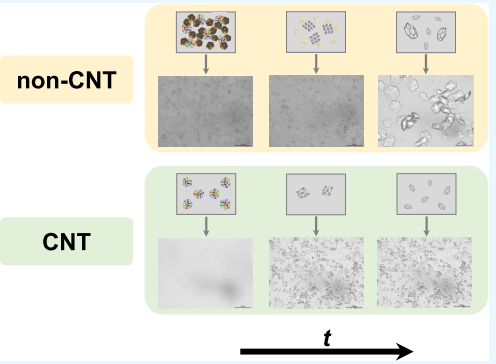

1. INTRODUCTION

Crystallization starts with nucleation, a first-order phase transition by which molecules pass from a wholly disordered state to an ordered one.[1] Small domains (i.e., nuclei) spontaneously appear during a homogeneous nucleation event, eventually evolving into a detectable crystal.[2] Protein nucleation requires extremely high supersaturation levels to overcome the critical free energy barrier. Introduced by Volmer and Weber in 1926, the *Classical Nucleation Theory* (CNT) is the most consensual theory to explain protein nucleation mechanisms. This classical approach describes nucleation as a process involving the formation of a critical nucleus and its subsequent growth.[3] One of the assumptions of the CNT is that all clusters exhibit the same crystallinity degree regardless of their size.[4] However, the validity of some of these assumptions has been questioned and even contradicted over the past 2 decades by different theories/observations, which can be resumed as follows.[5−8]

(i) **Experimental observations**: when the nucleation rate is much faster or slower than the one predicted by the CNT or when the observed nuclei size distribution differs significantly from the theoretical predictions.

(ii) **Thermodynamic calculations**: when the thermodynamic calculations (e.g., free energy barrier) are much different compared to the values predicted by the CNT or when the critical nucleus size significantly differs from the estimated value.

(iii) **Nonclassical nucleation theories**: when the existence of nonclassical nucleation pathways that do not involve the formation of a critical nucleus, which might suggest that the CNT does not fully describe the nucleation process.

A schematic representation of a protein crystallization process involving classical (CNT) versus non-classical perspectives of the nucleation mechanism can be observed in Figure 1.

The nonclassical approaches describe nucleation as a multistep process involving metastable intermediate states (i.e., precritical clusters). One of these nonclassical theories is the two-step nucleation theory proposed by Galkin and Vekilov in 2000[9] (lysozyme). Sleutel and van Driessche (2014)[5] showed evidence that clusters are *liquid-like* and metastable concerning the emerging crystalline phase (e.g., lysozyme and insulin). Ferreira et al. (2017)[10] demonstrated the existence of clusters

Received: December 15, 2023
Revised: March 29, 2024
Accepted: April 8, 2024
Published: May 13, 2024

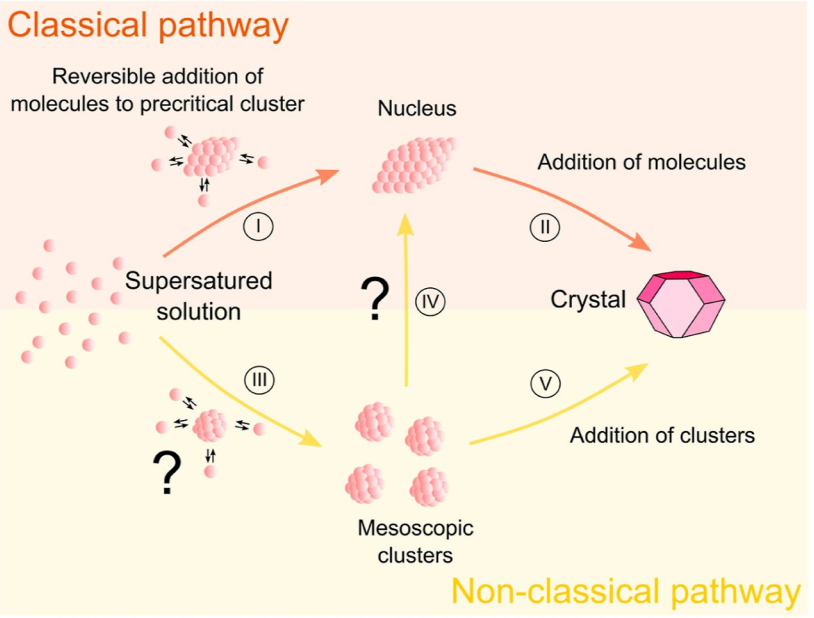

Figure 1. Overview of classical [(I)−(II)] and nonclassical [(III)−(V) or (III)−(IV)−(II)] nucleation pathways from a supersaturated protein solution to a crystalline phase [adapted from ref 5].

that do not give rise to crystals and remain in solution (lysozyme). Kaissaratos et al. (2021)[8] also stated that two-step nucleation is a phase transformation over the classical pathway due to a lower surface-free energy barrier. Mesoscopic insulin-rich clusters form in solution and facilitate the insulin nucleation process.[8]

One of the most widely used techniques to characterize nucleation mechanisms (e.g. early stages of crystallization and aggregation) is Dynamic Light Scattering (DLS). DLS detects in situ scattering intensity fluctuations due to the Brownian motion of particles,[11,12] which are related to particle size and polydispersity information.[13] Moreover, this optical technique allows to simultaneously determine the monodispersity of species of interest and the presence of soluble high-order assemblies and/or aggregates[14] as highlighted in the revision reported by Amin et al. (2014).[11] Insulin crystallizes in a hexameric form, while in solution, an equilibrium mixture of monomers, dimers, tetramers, hexamers, and possibly higher associated states occurs.[15] Additionally, acid solutions (e.g., HCl) and metallic ions (e.g., Zn^{2+}) and insulin molecules tend to form dimers[16,17] and hexamers,[18,19] respectively.

Several authors have reported studies about the behavior of proteins (e.g., lysozyme and serum albumin) and monoclonal antibodies (e.g., immunoglobulin) in solution using DLS. First, Bohidar (1998)[20] conducted assays and observed equilibrium aggregate formation, even at very low insulin concentrations (0.04−0.15 mg mL^{-1}). Li et al. (2011)[21] monitored aggregation in concentrated lysozyme solutions(<200 mg mL^{-1}) and determined the size of clusters, which provided further insights into complex cluster formation scenarios. Amin et al. (2012)[22] detected changes in denatured serum albumin solutions associated with the appearance of insoluble aggregates at high temperatures (60−80 °C) through an optimized DLS optical microrheology setup. Pathak et al. (2013)[23] performed experiments with a monoclonal antibody (immunoglobulin, 10 and 107 mg mL^{-1}) and concluded that monomers and reversible clusters coexist in solution. Nicoud et al. (2015)[24] monitored the kinetics of aggregate growth (i.e., size and morphology) of monoclonal antibody solutions (immunoglobulin, <60 mg mL^{-1}). More recently, Dharmaraj et al. (2016)[25] studied an extended range of lysozyme concentrations, and three different scenarios were reported at a low-temperature value (5 °C): (1) at low concentrations (∼1 mg mL^{-1}), the hydrodynamic radius corresponded to one of a monomer; (2) at intermediate concentrations (∼150 mg mL^{-1}), a decrease in the apparent hydrodynamic radius was captured due to increased repulsions between the monomers; and (3) at high concentrations (∼473 mg mL^{-1}), attractions, clustering, and hydrodynamic effects slow the diffusion, and the hydrodynamic radius increased. Last, Gonçalves et al. (2016)[26] distinguished the presence of different oligomers (monomeric species with a small percentage of dimeric and trimeric species) during the assays performed with serum albumin (1 mg mL^{-1}).

The main goals of this work are (i) to characterize the rheology of insulin solutions in the presence of variable precipitant solution concentrations at a broad temperature range (5−40 °C), (ii) to analyze the insulin behavior in solution using different characterization techniques [Dynamic Light Scattering (DLS), Energy-Dispersive Spectroscopy (EDS), Scanning Electron Microscopy (SEM), and Differential Scanning Calorimetry (DSC)], and (iii) to provide a further understanding of the insulin nucleation mechanisms, which includes classical and nonclassical pathways. Thus, the results can be divided into three main parts: (I) crystal formation following the CNT mechanism, where the nuclei are formed and grow until reaching a detectable size (crystal); (II) multistep nucleation mechanism (non-classical CNT) governs the crystallization process as crystal appearance seems to require the presence of initially formed aggregates; and (III) aggregate formation with no evolution to a crystalline phase.

Different research teams have presented nonclassical pathways to describe protein nucleation as highlighted by the reviews reported by Vekilov (2004),[6] Karthika et al. (2016),[27] Sleutel and van Driessche (2018),[4] Gebauer et al. (2018),[28] Jin et al. (2020),[29] Zhang et al. (2021),[30] and Warzecha et al. (2021).[31] Insulin is a unique case of benign in vivo crystallization with

https://doi.org/10.1021/acsomega.3c10052
ACS Omega 2024, 9, 23364−23376

relevant biological functions.[8] However, only two studies reported nonclassical perspectives of insulin crystals: Sleutel and van Driessche (2014)[5] and Kaissaratos et al. (2021).[8] Therefore, to the best of our knowledge, the current study constitutes the first work describing nonclassical pathways associated with shear-induced insulin crystallization events. An overview of the reported literature involving the rheological investigation of proteins and antibodies was published elsewhere by Ferreira et al. (2022).[32]

2. EXPERIMENTAL SECTION

2.1. Protein Solution Preparation. The studied protein was recombinant human insulin (Sigma-Aldrich, 5808 g mol^{-1}, CAS-no. 11061-68-0). The solution preparation protocol was previously reported by Ferreira et al. (2002)[33] and Ferreira et al. (2022),[32] which includes the following: (i) insulin solution [0.25 and 2.5 mg mL^{-1} (pH = 1.6)] and (ii) precipitant solution [composed of 6.25 mM zinc chloride (Sigma-Aldrich, CAS-no. 7646-85-7), 62.5 mM trisodium citrate (Sigma-Aldrich, CAS-no. 6132-04-3), and 12.5% (v/v) acetone (VWR International, CAS-no. 67-64-1) (pH = 6.2)]. There are several experimental protocols to crystallize insulin, not only in terms of cosolvents (e.g., acetone and phenol) but also in zinc-providing salts (e.g., chloride, sulfate, and acetate). Chen et al. (2017)[34] and Hodzhaoglu et al. (2016)[35] highlighted the importance of cosolvents to obtain well-formed insulin crystals without face defects.

2.2. Rotational Rheology Experiments. Shear viscosity curves were measured using a stress-controlled shear rheometer (Physica MCR301, Anton Paar) with a minimum resolvable torque of M_{min} = 0.1 μN m equipped with a cone-and-plate (CP) geometry to ensure a uniform shear rate profile.[36] The temperature control was done through an integrated Peltier temperate system set at the studied temperature value (5−40 °C). Moreover, a solvent trap was used to minimize the solvent evaporation. However, sample evaporation was still observed under extreme experimental conditions [low precipitating agent concentration (1.6 mM zinc chloride) and high temperature (40 °C) in assays taking more than 60 min] promoting aggregate/agglomerate formation. The rheological assays were performed at fixed insulin (2.5 mg mL^{-1}, C_p) and variable precipitating agent (1.6−4.7 mM) concentrations based on previous work from the research team,[32] which corresponds to a supersaturation ratio ($S = C_p/C_s$, where C_s is the protein solubility concentration) range of 85−140 at 20 °C. The solutions were placed in a thermostatic bath (Huber—Ministat 125, accuracy ± 0.02 °C) at a set value (5−40 °C) for 30 min prior to the measurement. After this time, the samples (precipitant solution followed by insulin solution, pH = 6.2) were pipetted to the rheometer. This procedure ensured no temperature gradients during the mixing procedure, which could eventually lead to uncontrolled nucleation or aggregation/agglomeration events. Further details about the rheometer apparatus, experimental setup, and methodology can be found elsewhere.[32] The protein samples were initially presheared for 25 min at a shear rate high enough to ensure a homogeneous mixture while avoiding any protein denaturation event ($\dot{\gamma} = 5 \times 10^2\ s^{-1}$). Denaturation due to high shear rates is only expected to occur at $\dot{\gamma} > 10^7\ s^{-1}$.[23] The steady-state shear rheology was characterized by descending $[\downarrow \dot{\gamma}(t)]$ shear rate sweep measurements within $10^{-4} \leq \dot{\gamma}\ [s^{-1}] \leq 10^3$ expressed in a linear ramp (Δt = 60 min). Last, at least three independent experiments were carried out to ensure data reproducibility.

2.3. Optical Microscopy. Sheared samples were collected at the end of each rheological measurement in an Eppendorf tube (1.5 mL), stored at room temperature (22 ± 2 °C), and periodically observed (up to 15 days) to capture the presence and/or evolution of crystals and/or aggregates/agglomerates. This procedure was carried out using a microscope (DMI5000 M, Leica Microsystems CMS GmbH) equipped with a digital camera (DFC350 FX, Leica Microsystems CMS GmbH). The analysis was performed by *LAS v3.7.0* software (*Leica Application Suite*).[37]

2.4. Dynamic Light Scattering. DLS measurements were done using an ALV/DLS−5000F instrument equipped with an SP-86 goniometer system (ALV-GmbH, Langen, Germany) and a continuous-wave diode-pumped Nd/YAG solid-state Compass-DPSS laser with a symmetrizer (Coherent Inc., Santa Clara, CA). The laser operates at a wavelength of 488 nm with an output power of 75 mW. The intensity scale was calibrated against the scattering from toluene. Samples of mixed freshly prepared protein and precipitant solutions were incubated in glass cuvettes (1.0 mL) at fixed temperature values (5−40 °C: wavevectors around 0.02 nm^{-1}) and periodically analyzed at a scattering angle of 90° to the incident beam. Last, the DLS samples were diluted to a sufficiently low insulin concentration (0.25 mg mL^{-1})[24] both in the absence and presence of the precipitant solution at variable concentrations (1.6, 3.1, and 4.7 mM) and temperature (5, 20, and 40 °C). The analysis was also performed for different incubation times (up to 6 h) to characterize the insulin behavior in solution and to explore the equilibrium between the different oligomeric forms over time.

In a DLS experiment, the first-order correlation function $[g_1(\tau)]$ decays exponentially and is dependent on a decay constant (Γ [s^{-1}]) for macromolecules undergoing a Brownian motion (eq 1).[38]

$$g_1(\tau) = \exp(-\Gamma\tau) \tag{1}$$

where τ [s] is the lag time. The decay constant (Γ, eq 1) is directly related to the diffusion coefficient of insulin (D_τ [$m^2\ s^{-1}$]) (eq 2).[38]

$$\Gamma = D_\tau q^2 \tag{2}$$

where q [m^{-1}] is the Bragg wave vector which is proportional to the solvent (diluted HCl solution) refractive index (n [—] = 1.3331) (eq 3).[38]

$$q = \frac{4\pi n}{\lambda}\sin\left(\frac{\theta}{2}\right) \tag{3}$$

where λ [m] is the wavelength of incident light (488 nm) and θ [rad] the angle at which the detector is placed (90°).

Last, the hydrodynamic radius (R_h [m]) can be calculated by the Stokes−Einstein equation (eq 4). The hydrodynamic radius is defined as the radius of a hypothetical sphere that diffuses at the same rate as the crystals under investigation.[38]

$$D_\tau = \frac{k_B T}{6\pi\eta R_h} \tag{4}$$

where k_B [kg $m^2\ s^{-2}\ K^{-1}$] is the Boltzmann coefficient (1.38×10^{-23} kg $m^2\ s^{-2}\ K^{-1}$), T [K] is the temperature, and η [Pa s] is the shear viscosity of the solvent (diluted HCl solution).

2.5. Energy Dispersive Spectroscopy and Scanning Electron Microscopy. EDS analysis and SEM imaging were performed using a high-resolution scanning electron microscope with X-ray microanalysis: JEOL JSM 6301F/Oxford INCA

https://doi.org/10.1021/acsomega.3c10052
ACS Omega 2024, 9, 23364−23376

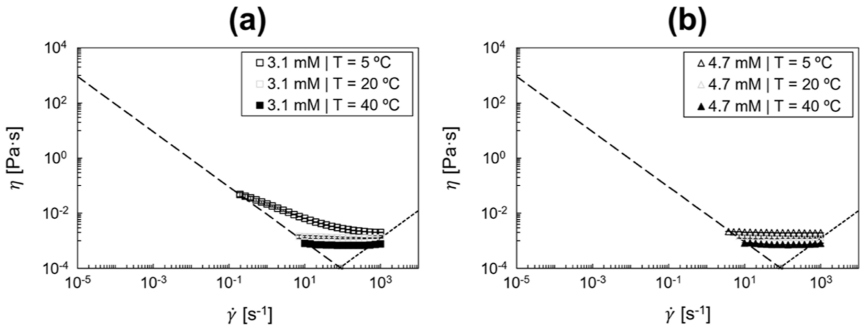

Figure 2. Steady-shear viscosity (η) as a function of the shear rate ($\dot{\gamma}$) measured in the temperature range of 5−40 °C during descending shear rate sweep experiments with fixed insulin concentration (2.5 mg mL^{-1}) and variable precipitating agent ($ZnCl_2$) concentrations: (a) 3.1 mM and (b) 4.7 mM. The dashed lines represent (i) the minimum measurable shear viscosity based on 10× the minimum resolvable torque and (ii) the onset of secondary flow due to Taylor instabilities [the bars indicate standard deviations from at least three independent experiments].

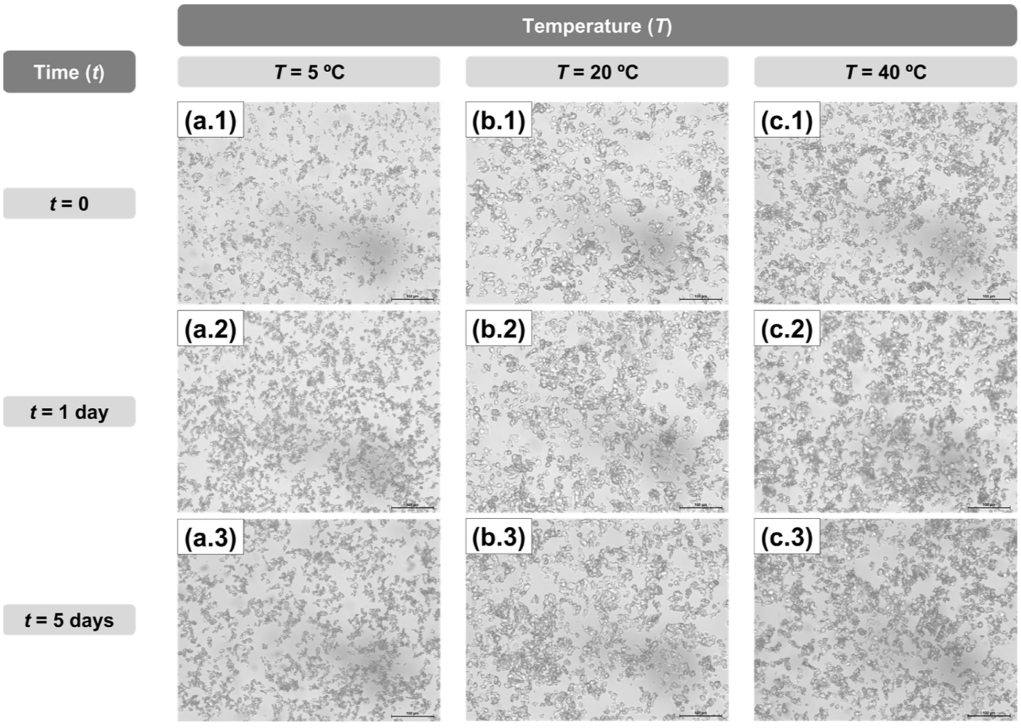

Figure 3. Representative samples from the rheological experiments with a duration of 60 min at (a) 5, (b) 20, and (c) 40 °C after (1) 0, (2) 1, and (3) 5 days: insulin concentration of 2.5 mg mL^{-1} and a precipitating agent ($ZnCl_2$) concentration of 3.1 mM [the indicated scale bars correspond to a length of 100 μm].

Energy 350. The samples collected after each rheological assay were dried under vacuum and coated with a Au/Pd film by sputtering for 100 s with a constant current value of 15 mA using the SPI module coater equipment. Last, the conditions in which images and the spectrum were obtained are indicated in the, respective, labels. EDS was employed to identify which chemical elements were present in the rheological samples at the studied precipitant solution concentration values (1.6−4.7 mM) and insulin concentration and temperature values of 2.5 mg mL^{-1} and 20 °C, respectively.

2.6. Differential Scanning Calorimetry. A SETARAM DSC-III heat flux microcalorimeter with Hastelloy batch vessels (900 μL) was used to determine the thermal behavior of insulin solutions (0.25 mg mL^{-1}). Temperature scans between 20 and 45 °C at 0.1 °C min^{-1} heating rate were performed. The measurements were carried out during two heating steps. Enthalpograms were analyzed by using *Calisto SETARAM* software. At least three independent experiments were carried out to ensure data reproducibility.

3. RESULTS AND DISCUSSION

Descending [$\downarrow \dot{\gamma}(t)$] shear rate sweep measurements were carried out at a fixed insulin concentration (2.5 mg mL^{-1}) in the presence of variable precipitant solution concentrations (1.6−4.7 mM) and temperature range (5−40 °C). At the end of each rheological assay, two distinct scenarios were obtained: (Shear-Induced Crystallization States) crystallization states following classical nucleation pathways and (Shear-Induced Aggregation/Agglomeration States) aggregation/agglomeration states, which will eventually evolve into crystallization states following nonclassical theories. The samples were followed for several hours and days (up to 15 days) by using optical microscopy.

3.1. Shear-Induced Crystallization States. The shear rate ($\dot{\gamma}$) dependence of the shear viscosity (η) at the studied

https://doi.org/10.1021/acsomega.3c10052
ACS Omega 2024, 9, 23364−23376

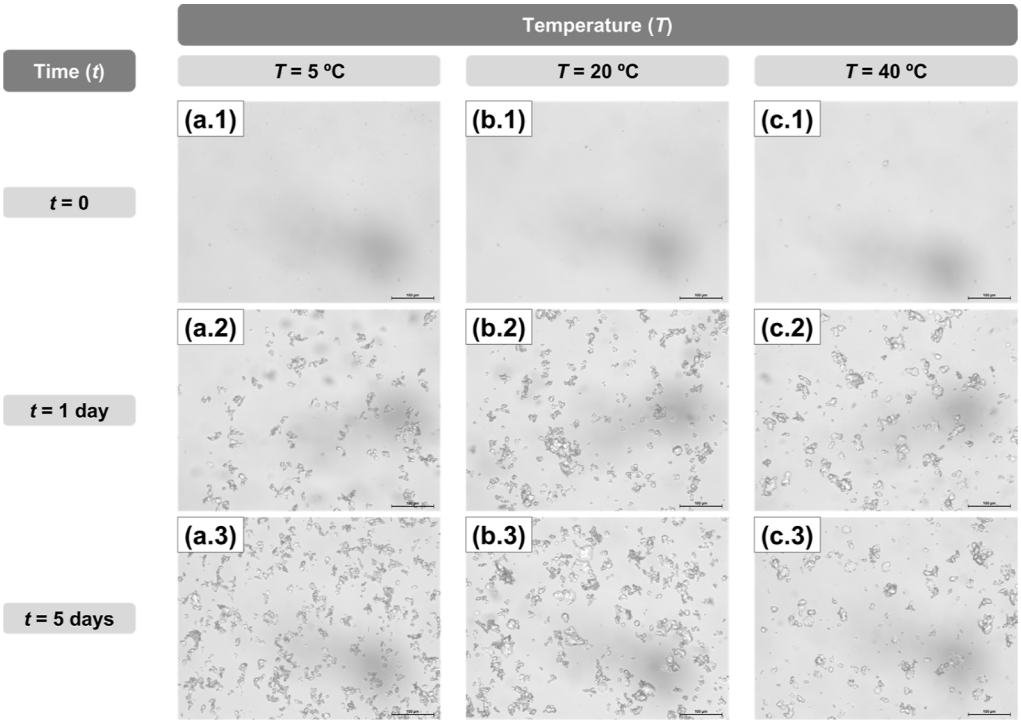

Figure 4. Representative samples from the rheological experiments with a duration of 60 min at (a) 5, (b) 20, and (c) 40 °C after (1) 0, (2) 1, and (3) 5 days: insulin concentration of 2.5 mg mL^{-1} and a precipitating agent ($ZnCl_2$) concentration of 4.7 mM [the indicated scale bars correspond to a length of 100 μm].

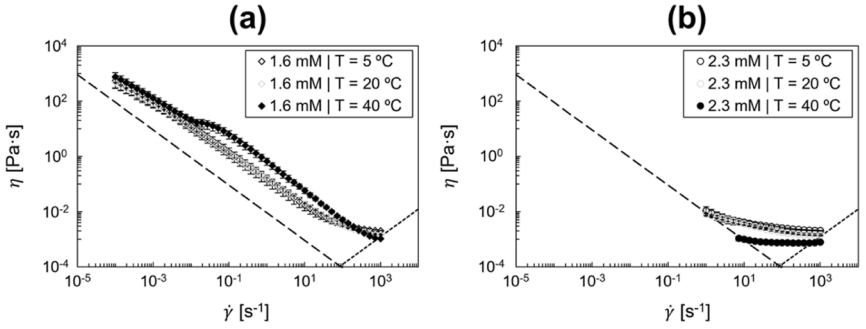

Figure 5. Steady-shear viscosity (η) as a function of the shear rate ($\dot{\gamma}$) measured in the temperature range of 5−40 °C during descending shear rate sweeps experiments with fixed insulin concentration (2.5 mg mL^{-1}) and variable precipitating agent ($ZnCl_2$) concentrations: (a) 1.6 mM and (b) 2.3 mM. The dashed lines represent (i) the minimum measurable shear viscosity based on 10× the minimum resolvable torque and (ii) the onset of secondary flow due to Taylor instabilities [the bars indicate standard deviations from at least three independent experiments].

precipitating agent concentrations (3.1 and 4.7 mM) and temperature range (5−40 °C) is presented in Figure 2, while the outcome of the shear-induced experiments over different days (up to 5 days) can be observed in Figure 3 and 4. At a moderate concentration of precipitating agent (3.1 mM), the transition from a shear-thinning behavior (low temperature) to Newtonian behavior (high temperature) is captured at 20 °C (Figure 2a), which is in accordance with a previous study.[32] At the highest precipitating agent concentration (4.7 mM), a Newtonian response and similar shear viscosity values are observed, regardless of the studied temperature value (Figure 2b).

Initially, rhombohedral insulin crystals[35] are formed at a moderate concentration of the precipitating agent (3.1 mM) (t = 0, Figure 3). The crystals are larger at high temperatures ($T \geq 20$ °C), while a high number of smaller crystals are produced at low temperatures (T = 5 °C). For this latter temperature, a visible increase in the shear viscosity is also observed [Figure 2a], which might be explained by the random insulin molecular distribution in the presence of many tiny crystals, thus contributing to increased flow resistance.

At high temperatures ($T \geq 20$ °C), the larger crystals might contribute to the molecular alignment of insulin molecules and, consequently, lower shear viscosities by a decreased flow resistance at the solvent molecular level. There is an indirect contribution in protein−solvent interaction due to the formation of larger crystals, which reduces the solvent accessible surface area of insulin molecules. Although no substantial crystal growth occurs at high temperatures ($T \geq 20$ °C), visible growth and appearance of new crystals take place over time (Figure 3, t = 1 and t = 5 days) at low temperatures (T = 5 °C). No detectable or very tiny crystals are initially observed at a high concentration of the precipitating agent (4.7 mM) (t = 0, Figure 4). This outcome might justify the Newtonian response [$\eta(\dot{\gamma}) \sim 10^{-3}$ Pa s] characteristic of the studied temperature

https://doi.org/10.1021/acsomega.3c10052
ACS Omega 2024, 9, 23364−23376

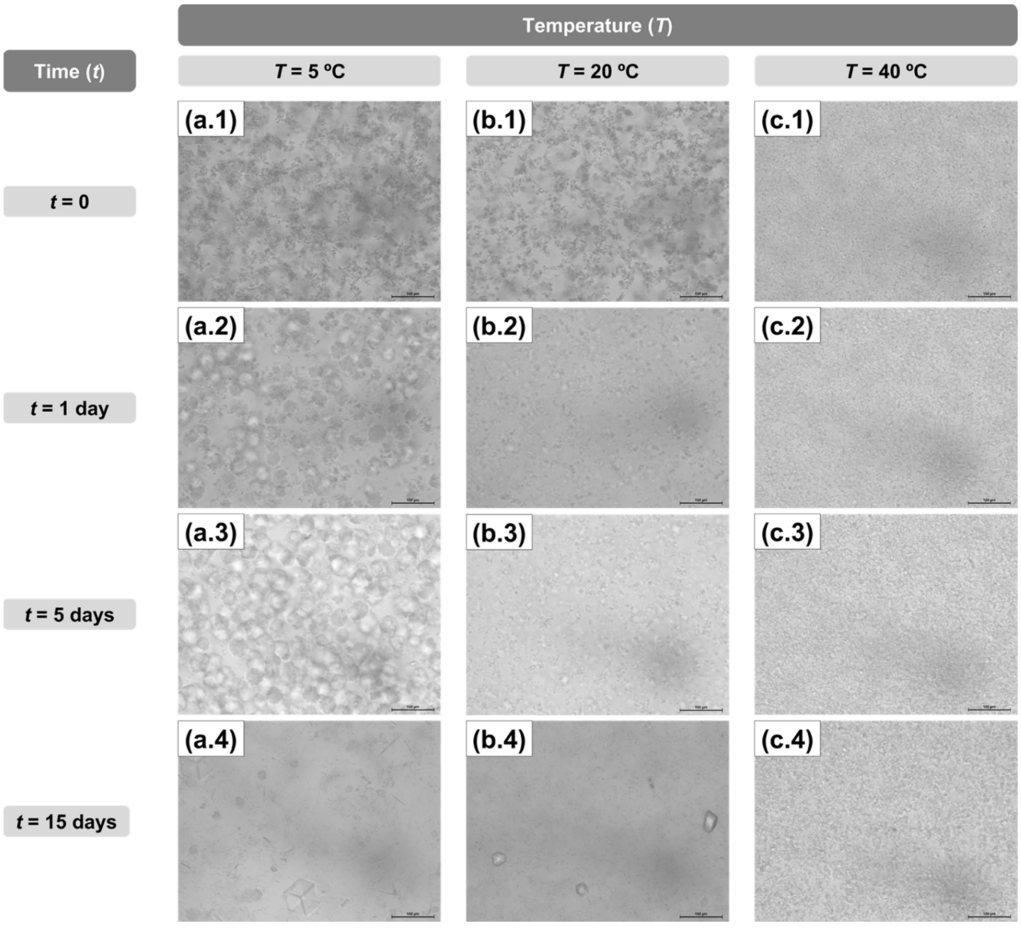

Figure 6. Representative samples from the rheological experiments with a duration of 60 min at (a) 5, (b) 20, and (c) 40 °C after (1) 0, (2) 1, (3) 5, and (4) 15 days: an insulin concentration of 2.5 mg mL^{-1} and a precipitating agent ($ZnCl_2$) concentration of 1.6 mM [the indicated scale bars correspond to a length of 100 μm].

range [Figure 2b]. Time-dependent rheological assays at a constant shear rate ($\dot{\gamma}$ = 200 s^{-1}) performed in a previous study showed no rheopectic effects.[32] After 1 day (t = 1 day, Figure 4), insulin rhombohedral crystals are formed at all of the studied temperature values, which are slightly larger at the highest temperature (T = 40 °C). Visible crystal growth and formation of new crystals occur at $T \leq$ 20 °C (t = 5 days, Figure 4).

3.2. Shear-Induced Aggregation/Agglomeration States. The rheological behavior of insulin solutions in the presence of the precipitating agent with concentrations (1.6 and 2.3 mM) and temperature range (5−40 °C) promoting aggregation/agglomeration events is presented in Figure 5. The outcomes of rheometry experiments over different days (up to 15 days) are listed in Figures 6 and 7. An evident shear-thinning response is observed in most cases, except at high temperatures (T = 40 °C) and intermediate precipitating agent concentration (2.3 mM), where Newtonian behavior appears [Figure 5b]. Moreover, temperature-independent shear viscosity at $\dot{\gamma} < 100\ s^{-1}$ and $T \leq$ 20 °C is observed for both precipitating agent concentrations (Figure 5).

At the lowest concentration of the precipitating agent (1.6 mM), noncrystalline structures are initially (t = 0) observed for the studied temperature range (5−40 °C). Dispersed aggregates/agglomerates are clearly visible at low temperatures ($T \leq$ 20 °C), while a more tightly packed solution is exhibited at 40 °C (Figure 6). These distinct outcomes are also observed in the rheological behavior. Although a yield stress behavior is exhibited for all the temperature values, with the shear viscosity ranging more than 6 orders of magnitude (*solid-like* behavior, where the insulin solutions are almost not flowable), the shear viscosity curves differ for the analyzed temperature range [Figure 5a] as follows.

- At low temperatures ($T \leq$ 20 °C), the curves are similar, which is in accordance with the similar observed aggregation/agglomeration (Figure 6 at t = 0). The insulin solutions become less cloudy (i.e., turbid), and the aggregates/agglomerates tend to rearrange in solution over time (Figure 6 at t > 0). This rearrangement is even more evident after longer times at the lowest temperature value (T = 5 °C), which seem to lead to the formation of aggregated clusters (Figure 6 at t = 5 days).

The first crystals appear in solution after 15 days in the form of either single rhombohedral crystals in a cloudy solution at T = 20 °C or simultaneously single large rhombohedral and needle-shaped crystals in the presence of discrete aggregates/agglomerates at T = 5 °C (Figure 6 at t = 15 days).

- At high temperatures (T = 40 °C) and high shear rates ($\dot{\gamma}$ > 200 s^{-1}), the shear viscosity values are lower compared to the values obtained at low temperatures ($T \leq$ 20 °C) [Figure 5a] by following the Arrhenius equation.[39−41] Conversely, at lower shear rates ($\dot{\gamma}$ < 200 s^{-1}), the shear viscosities are higher than those at low temperatures ($T \leq$ 20 °C), which is probably due to the

https://doi.org/10.1021/acsomega.3c10052
ACS Omega 2024, 9, 23364−23376

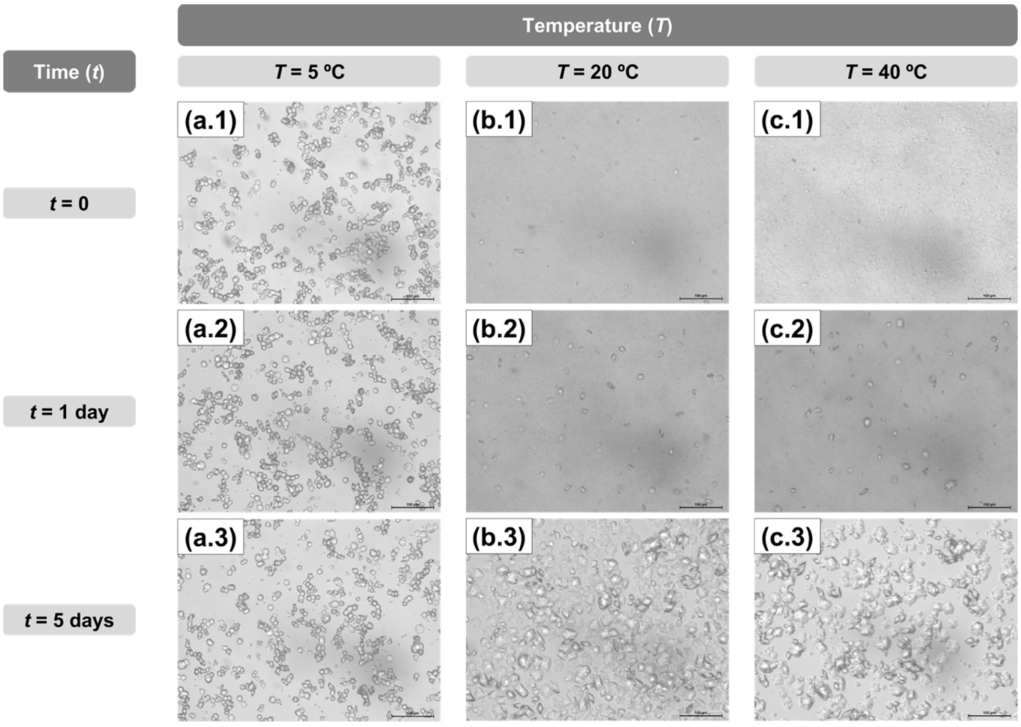

Figure 7. Representative samples from the rheological experiments with a duration of 60 min at (a) 5, (b) 20, and (c) 40 °C after (1) 0, (2) 1, and (3) 5 days: an insulin concentration of 2.5 mg mL^{-1} and a precipitating agent ($ZnCl_2$) concentration of 2.3 mM [the indicated scale bars correspond to a length of 100 μm].

formation of irreversible and insoluble aggregates/agglomerates during the rheological experiment [Figure 5a]. Additionally, a visible decrease in the increasing shear viscosity rate is registered at very low shear rates ($\dot{\gamma} \sim 10^{-2}$ s^{-1}).

Time-dependent rheological assays at a constant shear rate ($\dot{\gamma}$ = 200 s^{-1}) performed in a previous study showed no rheopectic effects.[32] This behavior might indicate that the maximum level of closed-packed organization has been reached. At this point ($\dot{\gamma} < 10^{-2}$ s^{-1}), a temperature-independent shear viscosity response is captured [Figure 5a]. No significant changes are observed in the final samples over time, even after several days (Figure 7 at t = 15 days) [Figure 5a].

High temperatures are prone to insulin aggregation and denaturation in acidic solutions.[20] However, no denaturation events were observed for the conditions promoting aggregation and agglomeration, including the highest measured temperature value (40 °C). Pathak et al. (2013)[23] highlighted that irreversible clusters contribute to shear viscosity increases of immunoglobulin solutions, especially at low shear rates due to nonequilibrium cluster formation.[23] Castellanos et al. (2014)[42] performed experiments with monoclonal antibody solutions and observed aggregate formation at 40 °C, which exhibited a yield stress response.[42] Amin et al. (2014)[43] reported that shear viscosity increases are associated with the formation of insoluble aggregates (i.e., nonequilibrium systems), particularly at low shear rates.[43] Nicoud et al. (2015)[24] studied the impact of aggregate formation on the changes in shear viscosity of concentrated monoclonal antibody solutions. These authors concluded that the viscosity of an aggregated protein solution is lower than that of a monomeric protein solution with a similar occupied volume fraction, probably due to a polydisperse aggregate distribution.[24] To further understand the significant decrease in the increasing shear viscosity rate at $\dot{\gamma} \leq 10^{-2}$ s^{-1}, additional rheological assays were carried out at fixed shear rates over time. The main results and discussion are provided in Supporting Information, S1.

At an intermediate concentration of the precipitating agent (2.3 mM), the largest rhombohedral crystals among all of the studied experimental conditions are initially obtained at the lowest temperature (T = 5 °C). In contrast, a few small crystals in the presence of cloudy solutions with visible aggregates/agglomerates are produced at high temperatures ($T \geq 20$ °C) (Figure 7 at t = 0). Although aggregates/agglomerates are initially observed at $T \geq 20$ °C (Figure 7), the shear viscosity range values are not as high as the values obtained at the lowest concentration of the precipitating agent (1.6 mM) (Figure 5). Therefore, the presence of crystals seems to contribute to a reduction of the shear viscosity.

A temperature-independent shear viscosity is captured at $T \leq 20$ °C ($\dot{\gamma} < 100$ s^{-1}), where the formation of aggregates/agglomerates is probably favored [Figures 5b and 8 at t = 0]. No new nucleation events and crystal growth seem to take place over time at T = 5 °C (Figure 7). At high temperatures ($T \geq 20$ °C), new rhombohedral crystals appear and grow in solution, while the aggregates/agglomerates tend to disappear, and the solution becomes less turbid (Figure 7 at $t \geq 1$ min). After 5 days, the larger rhombohedral crystals are obtained at $T \geq 20$ °C (Figure 7 at t = 5 min).

DLS experiments were performed to explore the role of zinc in the insulin crystallization and aggregation and agglomeration states and the equilibrium between the different oligomeric forms. Besides these experiments, circular dichroism (CD) and DSC measurements were carried out to understand the protein behavior at high temperatures (40 °C). The main results are presented along subsection (Insulin Behavior in Solution). Last, a detailed discussion involving all of the obtained results is

https://doi.org/10.1021/acsomega.3c10052
ACS Omega 2024, 9, 23364−23376

provided along subsection (Overview of the Results), which also includes the main results from the EDS analysis and SEM imaging.

3.3. Insulin Behavior in Solution. The intensity distribution [%] as a function of the hydrodynamic radius [R_h] for insulin solutions in the absence of precipitant solution at different temperature values is displayed in Figure 8. No significant changes in the intensity distribution were observed after t = 2 h. Thus, the analysis was not performed for a longer time.

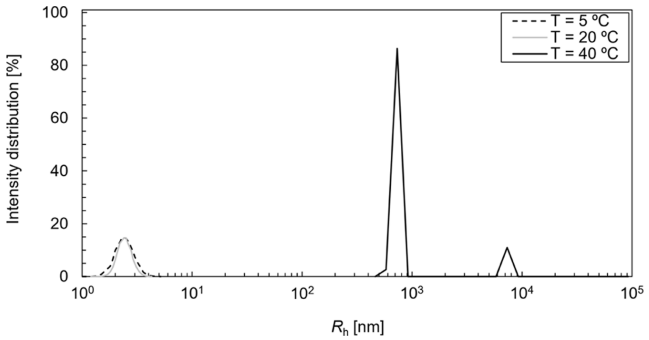

Figure 8. Hydrodynamic radius distribution at different temperatures and fixed insulin concentration (0.25 mg mL^{-1}) in the absence of a precipitant solution.

At low temperatures (5 and 20 °C) in the absence of a precipitant solution, the insulin solutions exhibit a homogeneous distribution, which is characterized by a single peak (Figure 8). The average hydrodynamic radius is around 2.45 nm (diffusion coefficients of 5.1×10^{-11} m^2 s^{-1} and 8.13×10^{-11} m^2 s^{-1} at 5 and 20 °C, respectively), thus suggesting that insulin is highly hexameric[44] (Figure 8). The data presented in the literature is consistent with the predictions of the current study. Link and Heng (2022)[45] (insulin concentration values below 1 mg mL^{-1}) and Jensen et al. (2014)[46] (insulin concentration around 0.6 mg mL^{-1}) obtained a hydrodynamic radius below 3 nm and a diffusion coefficient around 1×10^{-10} m^2 s^{-1}. Yousefi et al. (2016)[47] (insulin concentration of 0.2 mg mL^{-1}) reported values for the hydrodynamic radius around 1 nm.

At high temperatures (40 °C), oligomeric forms and/or aggregates/agglomerates are pointed out by the appearance of two distinct peaks at around 0.7 and 7 μm. The single-peak distribution is recovered by lowering the temperature, which might suggest reversible structural changes. The suspicious doubts about the insulin behavior at 40 °C and the possible formation of amyloid fibrils can be discerned through CD spectroscopy.[48] Amyloid fibrils consist of the partial unfolding of the insulin structure and, consequently, changes in the CD spectra, which indicate the extensive conversion of the molecular conformation from α-helical to β-sheet structures.[49] In a previous study, CD measurements performed at 20 °C revealed a reduction of α-helical content, while excluding the appearance of structures rich in β-sheets or random coils.[33] CD experiments conducted at 40 °C revealed no significant changes in the secondary structure of insulin when compared to the results at 20 °C (Supporting Information, S2). Attending to the available literature for insulin, the formation of amyloid fibbers only occurs at temperatures higher than 60 °C.[49−51] The DSC data from the consecutive heating steps are displayed in Figure 9a, while Figure 9b represents the first-order correlation functions before and after the heating steps (measurements performed at 20 °C).

The DSC data reveal that the heat flow during the two consecutive heating steps significantly differs over the studied temperature range. The exothermic behavior observed during the second heating step is similar compared to the first one until temperatures within the range of 25−30 °C. At higher-temperature values, the heat flows of the second step are lower. This trend might indicate that aggregates are being formed [Figure 9a]. These results might suggest that irreversible aggregation is occurring, which seems to explain the observations during the rheological assays [Figures 5a and 6]. Before the insulin samples were exposed to the heating steps, insulin monomers (or eventually dimers) with small scatters seem to be present in solution. However, after the heating steps, the presence of oligomers is registered at longer times, which again suggests the presence of aggregates [Figures 8 and 9b]. To further investigate this distinct behavior at 40 °C, the DLS analysis was extended to an incubation time of 6 h.

The experimentally measured count rates and first-order correlation functions for the studied scenarios are shown in Figures S2−S8 (Supporting Information, S3). Moreover, DLS experiments were conducted at three different concentrations of precipitant solution (1.6−4.7 mM) and temperature values (5−40 °C), and the analysis was conducted over time. The main results are presented in Figures S10−S15 and Tables S1−S3 [Supporting Information, S3; see eqs 2 and 4].

For a precipitant solution concentration of 3.1 mM, the studied cases are characterized by single narrow peaks [Figures

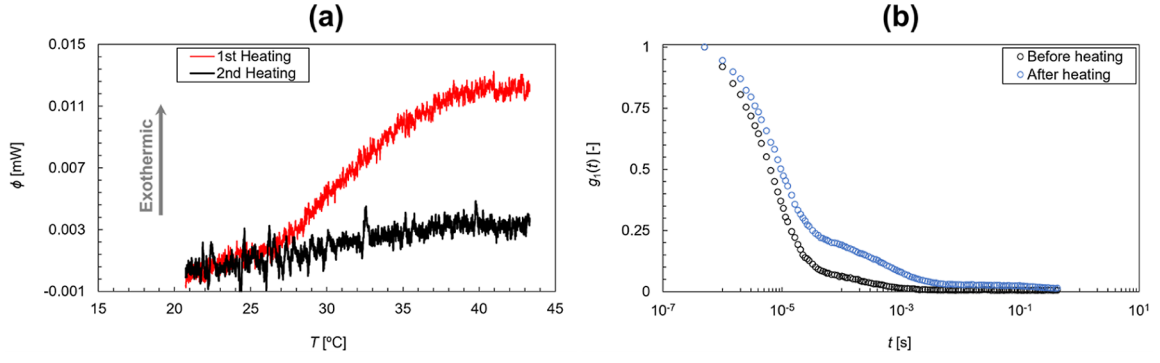

Figure 9. (a) Heat flow in function of temperature during two consecutive heating steps (arrow indicates the thermodynamic flow sign) and (b) normalized first-order correlation function in function of the lag time at 20 °C before and after the heating steps; fixed insulin concentration (0.25 mg mL^{-1}).

https://doi.org/10.1021/acsomega.3c10052
ACS Omega 2024, 9, 23364−23376

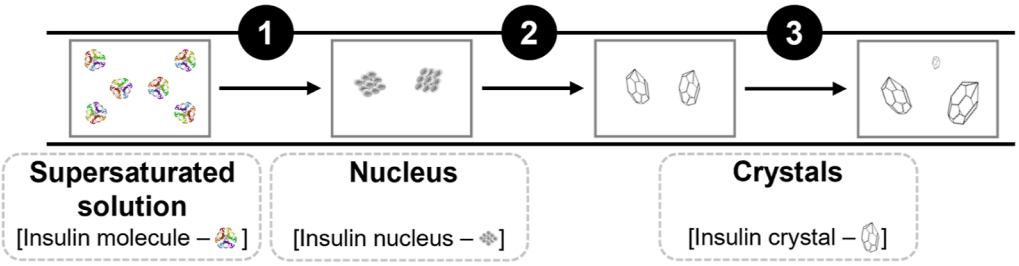

Figure 10. Schematic representation of the CNT pathway based on experimental evidence from the liquid bulk until the crystalline phase for precipitant solutions with concentrations of 3.1 and 4.7 mM.

S10−S12b]. For a high precipitant solution concentration (4.7 mM), the hydrodynamic size range seems to be located around 10^3−10^4 nm [Figures S10−S12c]. The hydrodynamic size distributions at low temperatures (5 °C) reveal two different aspects: the existence of two peaks for the incubation time (15 min) and the existence of narrower peaks for longer incubation times (2 and 3 h) [Figure S10c]. At high temperatures (40 °C), more than one peak is registered for some of the incubation times [Figure S12c]. Last, at low precipitant solution concentrations (1.6 mM), the hydrodynamic size range seems to be located around 10^2−10^3 nm. However, the hydrodynamic size distributions significantly differ along the incubation time [Figures S10−12a], which is especially clear at 40 °C [Figure S12a].

In the presence of zinc salts, Kadima et al. (1993)[52] reported that the hydrodynamic radii of the monomer, dimer, tetramer, and hexamer are 1.5, 2, 2.5, and 3 nm, respectively. Hvidt (1991)[53] obtained an average hydrodynamic radius of 5.6 nm, close to the crystallographic size of the insulin hexamer. More recently, Smith et al. (2012)[54] (insulin concentrations below 5 mg mL^{-1}) concluded that insulin monomers with an average hydrodynamic radius of 2 nm are formed in the presence of sodium chloride. Last, insulin forms hexamers in the presence of zinc salts even at insulin concentrations below 0.1 mg mL^{-1}.[46]

On the one hand, for all the studied temperatures (5−40 °C), a fast decay of the first-order correlation function is observed for a precipitant solution concentration of 3.1 mM [Figures S13−S15b]. This observation is related to the appearance of monomers (below or around 1 nm), which contributes to small scattering differences and thus fast diffusion (high diffusion coefficients) (Tables S1−S3). On the other hand, a slow decay of the correlation function is observed for a precipitant concentration of 4.7 mM [Figures S13−S15c], regardless of the studied temperature value.

The correlation functions present fluctuations over the incubation time [Figures S13−S15c], which means large fluctuations in the average hydrodynamic size (Tables S1−S3). Except at 40 °C [Figure S15c], the absence of a baseline in the correlation functions might exclude the hypothesis of large particle formation [Figures S13c and S14c]. The large decay gradient indicates sample polydispersity [Figures S13−S15c]. Last, for a precipitant solution concentration of 1.6 mM, the studied cases exhibit correlation functions with slow decay [Figures S13a and S15a], except at 20 °C [Figure S14a]. This slow decay is translated into large average hydrodynamic sizes (Tables S1 and S3) and large sample polydispersity [Figures S13a and S15a]. The incubation time seems to play a critical role, as significant differences in both correlation functions [slower decays at longer incubation times: Figures S13a and S15a] and average hydrodynamic sizes (larger hydrodynamic sizes at longer incubation times: Tables S1 and S3) are registered. These observations might suggest aggregation and agglomeration events, especially at 5 °C (average hydrodynamic size larger than 100 μm) (Table S1).

Dharmaraj et al. (2016)[55] performed experiments with lysozyme and concluded that an additional slow mode appeared at high protein concentrations (150−473 mg mL^{-1}). This observation revealed that a simple exponential could not fit the first-order correlation function at low temperatures (5 °C). Pathak et al. (2013)[56] associated monomers with the smallest scatters and fastest diffusion during experiments conducted with immunoglobulin (10 and 107 mg mL^{-1}). Additionally, aggregation was characterized by large hydrodynamic sizes and the appearance of more than one peak. Amin et al. (2012)[57] observed narrow peaks while conducting experiments with BSA (2−10 mg mL^{-1}) at high-temperature values (60 and 80 °C), which indicated that the particles were well dispersed and not aggregated. Moreover, the authors captured a slight evolution to longer decay times. This behavior was attributed to the slow evolution of the protein structure with increasing incubation time.

3.4. Overview of the Results. For the studied experimental conditions (temperature and precipitant composition) along (3.1), the experimental findings support the CNT as each cluster, after reaching a critical size, leads to the formation of a crystal without the appearance of any intermediate stage (e.g., aggregate). These observations suggest homogeneous nucleation since nuclei are spontaneously generated through clusters, thus originating the crystals.[58,59] The CNT mechanism lies in two main assumptions: (i) prenucleation clusters are crystalline and (ii) clusters have a critical size. Even though the current experimental techniques [rheometry characterization—Figure 2 and optical microscopy—Figures 3 and 4, see subsection (Shear-Induced Crystallization States)] are unable to inspect the initial stages of nucleation, the crystallization outcome suggests the validity of the CNT's assumptions. Following the classical pathway to explain the experimental results, the proposed crystallization mechanism is highlighted in Figure 10.

For a precipitant solution concentration of 3.1 mM, the existence of single narrow peaks suggests the presence of well-dispersed particles (crystals) [Figures S10−S12b]. Crystal growth seems to be promoted at high temperatures ($T \geq 20$ °C) since larger hydrodynamic sizes are captured [Figures S11b and S12b]. These results entirely agree with the results presented in Figure 3, where larger insulin rhombohedral crystals are produced at high temperatures ($T \geq 20$ °C).

Except at 20 °C [Figure S11b], where significant differences in the hydrodynamic size distribution are observed as a function of the incubation time (probably due to the formation of new crystals), at the remaining temperatures values, no new particles

https://doi.org/10.1021/acsomega.3c10052
ACS Omega 2024, 9, 23364−23376

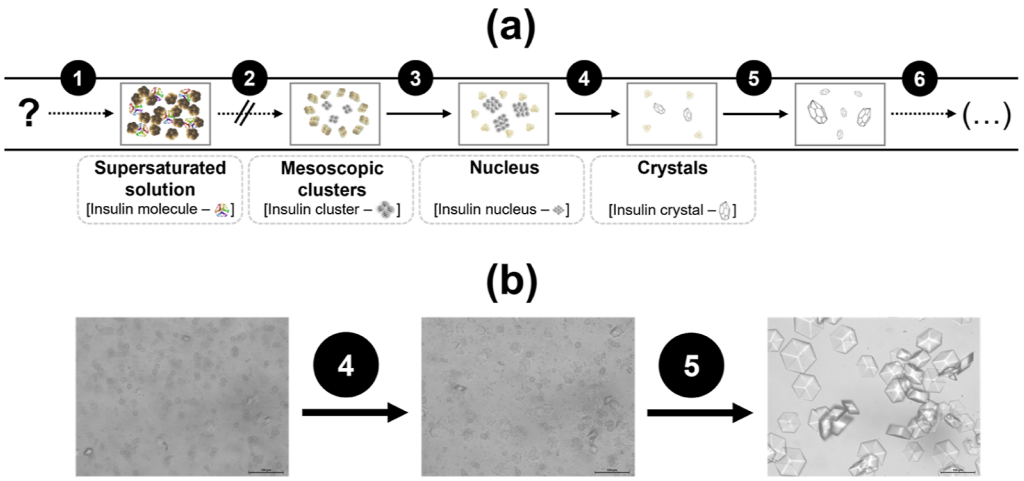

Figure 11. (a) Schematic representation of the proposed multistep nucleation mechanism based on experimental evidence from the liquid bulk until the crystalline phase with aggregate dissolution over time ['?' indicates the unknown initial stage and "(···)" the unfinished pathway] and (b) outcome of the rheological assay at different stages for precipitant solutions with a concentration of 2.3 mM.

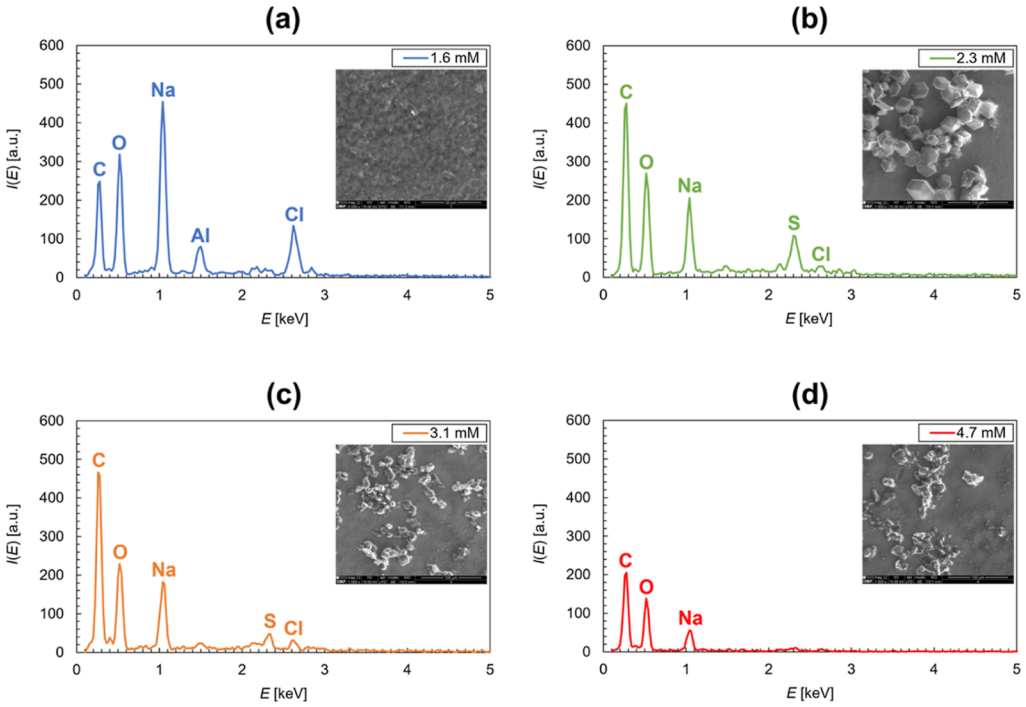

Figure 12. EDS profiles of the rheological samples performed at 20 °C with a fixed insulin concentration (2.5 mg mL^{-1}) and variable precipitating agent ($ZnCl_2$) concentrations: (a) 1.6, (b) 2.3, (c) 3.1, and (d) 4.7 mM. The figure insets are SEM images of the samples' regions of interest used for the EDS analysis.

seem to appear and/or no aggregation/agglomeration events seem to take place as no significant changes in the hydrodynamic size distributions are observed [Figures S10b and S12b]. These observations disagree with the shear-induced crystallization outcome as new crystals appear over time at low temperatures (T = 5 °C) (Figure 3). However, the rheological analysis also excludes the aggregation/agglomeration event hypothesis.

For a high precipitant concentration (4.7 mM), the hydrodynamic size distributions at low temperatures ($T \leq 20$ °C) reveal that more dispersed particles (crystals) form over the incubation time. Although two peaks are initially observed (incubation time of 15 min), at T = 5 °C, the peaks tend to be narrow after longer incubation times [Figure S10c], which might result in the formation of new crystals with no significant crystal growth. At T = 20 °C, broad hydrodynamic size distributions after long incubation times reveal sample polydispersity, which might result in the formation of new crystals [Figure S11c]. These outcomes are in accordance with the shear-induced assays as crystal growth and formation of new crystals are observed at $T \leq 20$ °C (Figure 4). At high temperatures (40 °C), crystal growth and/or formation of new crystals might occur as more than one peak is registered for some of the incubation times [Figure S12c]. The rheological assays reveal slightly larger crystals at this temperature over time (Figure 4).

For the studied experimental conditions (temperature and precipitant composition) along (Shear-Induced Aggregation/Agglomeration States), the non-classical multistep nucleation

https://doi.org/10.1021/acsomega.3c10052
ACS Omega 2024, 9, 23364−23376

theory might justify our observations since crystal formation seems to require the presence of initially formed aggregates/agglomerates. However, these aggregates/agglomerates tend to disappear over time (less cloudy solution) before the first crystals have started to be observed. On the one hand, these events suggest that nuclei might be formed within the mesoscopic protein clusters. On the other hand, these clusters might act as heterogeneous nucleation sites.[5] For this last case, the clusters proceed as catalysts, lowering the critical energy barrier by transforming clusters into nuclei. The proposed crystallization mechanism following a nonclassical pathway accompanied by experimental images is highlighted in Figure 11.

For low precipitant solution concentrations (1.6 mM), the hydrodynamic size distributions significantly differ along the incubation time [Figures S10−S12a]. This observation, together with the appearance of more than one peak for different incubation times at 20 °C [Figure S11a] and 40 °C [Figure S12a], suggests the formation of aggregates/agglomerates. Aggregation/agglomeration events and the, respective, formation of noncrystalline structures are captured during the shear-induced assays (Figure 7). However, these results reveal significant differences between low ($T \leq 20$ °C) and high ($T = 40$ °C) temperatures. Therefore, the DLS analysis is insufficient to justify the distinct behaviors: formation of dispersed aggregates/agglomerates and rearrangement over time ($T \leq 20$ °C) and tightly packed solution ($T = 40$ °C) (Figure 7).

DSC experiments were carried out, and the results revealed exothermic aggregation within the range of 25−30 °C during the two heating cycles. The fact that the exothermic signal during the second heating step is less intense compared to the one during the first cycle might indicate that the aggregation events are irreversible [Figure 9a]. Last, the samples collected after each rheological experiment were used to perform EDS assays for chemically characterizing the samples. The main results of the EDS analysis and SEM imaging are shown in Figure 12.

The EDS profiles reveal significant differences between shear-induced crystallization and shear-induced-aggregation/agglomeration events. At high insulin concentrations [Figure 12b−d], the most abundant chemical elements correspond to the peaks of carbon (insulin), oxygen (insulin), and sodium (buffer). Small peaks of sulfur (insulin) and chlorine (solvent and precipitant solution) might also appear [Figure 12b,c]. The SEM images reveal well-defined crystals with rhombohedral shape. At low insulin concentrations [Figure 12a], sodium is the most abundant chemical element followed by oxygen, carbon, chlorine, and aluminum. The presence of a significant amount of chlorine might be responsible for the aggregation and agglomeration events and absence of insulin crystals.

4. CONCLUSIONS

The interdisciplinary nature of this work builds up on the integration of rheological analysis, protein crystallization and aggregation/agglomeration experimentation, and characterization of the insulin behavior in solution for a broad temperature (5−40 °C) and precipitant ($ZnCl_2$) solution concentration (1.6−4.7 mM) ranges. First, crystallization events either follow the CNT or a nonclassical nucleation pathway (multistep nucleation mechanism). Although a typical Newtonian behavior (high precipitant solution concentrations: 3.1−4.7 mM) represents crystallization events in accordance with the CNT route, the nonclassical pathway is characterized by a transition from Newtonian to shear-thinning (intermediate precipitant solution concentrations: 2.3 mM). Second, aggregation/agglomeration events are characterized by a dominant shear-thinning response (low precipitant solution concentrations: 1.6 mM) with shear viscosity values ranging more than 6 orders of magnitude. Last, the employed characterization techniques (DLS, EDS, CD, and DSC) contribute to a significant understanding of the crystallization and/or aggregation and/or agglomeration mechanisms and might open new perspectives to crystallize other macromolecules (e.g., hard-to-crystallize proteins) in a more controlled manner.

The DLS analysis explores the equilibrium between different insulin oligomers over time and, consequently, extrapolates particle size distributions and polydispersity information, especially relevant in the context of aggregate/agglomerate formation. The EDS data identify the chemical elements present in solution and contribute to a better understanding between crystallization and aggregation/agglomeration events. Although the CD analysis is not able to detect changes in the insulin secondary structure at different temperature values, the DSC characterization determines the thermal behavior of the protein solutions, which reveals that irreversible aggregates are formed at high-temperature values (40 °C) and complements the DLS analysis. Moreover, aggregation events are characterized by lower heat flows.

■ ASSOCIATED CONTENT

Data Availability Statement

All data analyzed in this study are available through the manuscript and Supporting Information.

Supporting Information

The Supporting Information is available free of charge at https://pubs.acs.org/doi/10.1021/acsomega.3c10052.

Rheological analysis; CD spectroscopy; and DLS analysis (S3) (PDF)

■ AUTHOR INFORMATION

Corresponding Author

Joana Ferreira − *CEFT—Transport Phenomena Research Center, Department of Chemical Engineering, Faculty of Engineering, University of Porto, 4200-465 Porto, Portugal; ALiCE—Associate Laboratory in Chemical Engineering, Faculty of Engineering, University of Porto, 4200-465 Porto, Portugal;* Present Address: Department of Chemical Engineering, Massachusetts Institute of Technology, Cambridge, Massachusetts 02139, United States; orcid.org/0000-0002-7069-2693; Email: jmpferreira@fe.up.pt, joanaf@mit.edu

Authors

Vicente Domínguez-Arca − *Grupo de Física de Coloides y Polímeros, Departamento de Física de Partículas, Facultad de Física e Instituto de Materiales (iMATUS) e Instituto de Investigaciones Sanitarias (IDIS), Universidad de Santiago de Compostela, 15782 Santiago de Compostela, Spain; Grupo de Biosistemas e Ingeniería de Bioprocesos, Instituto de Investigaciones Marinas (IIM-CSIC), 36208 Vigo, Spain;* orcid.org/0000-0002-3500-5915

João Carneiro − *CEFT—Transport Phenomena Research Center, Department of Chemical Engineering, Faculty of Engineering, University of Porto, 4200-465 Porto, Portugal; ALiCE—Associate Laboratory in Chemical Engineering,*

https://doi.org/10.1021/acsomega.3c10052
ACS Omega 2024, 9, 23364−23376

Faculty of Engineering, University of Porto, 4200-465 Porto, Portugal

Gerardo Prieto − *Grupo de Física de Coloides y Polímeros, Departamento de Física de Partículas, Facultad de Física e Instituto de Materiales (iMATUS) e Instituto de Investigaciones Sanitarias (IDIS), Universidad de Santiago de Compostela, 15782 Santiago de Compostela, Spain;* orcid.org/0000-0002-3010-7197

Pablo Taboada − *Grupo de Física de Coloides y Polímeros, Departamento de Física de Partículas, Facultad de Física e Instituto de Materiales (iMATUS) e Instituto de Investigaciones Sanitarias (IDIS), Universidad de Santiago de Compostela, 15782 Santiago de Compostela, Spain;* orcid.org/0000-0002-2903-7857

João Moreira de Campos − *CEFT—Transport Phenomena Research Center, Department of Chemical Engineering, Faculty of Engineering, University of Porto, 4200-465 Porto, Portugal; ALiCE—Associate Laboratory in Chemical Engineering, Faculty of Engineering, University of Porto, 4200-465 Porto, Portugal*

Complete contact information is available at: https://pubs.acs.org/10.1021/acsomega.3c10052

Author Contributions

The manuscript was written through contributions of all authors. All authors have given approval to the final version of the manuscript. Joana Ferreira: conceptualization, methodology, investigation, and writing−original draft. Vicente Domínguez-Arca: methodology, investigation, and writing−review and editing. João Carneiro: methodology and writing−review and editing. Gerardo Prieto: methodology, investigation, and writing−review and editing. Pablo Taboada: methodology, investigation, and writing−review and editing. João Moreira de Campos: funding acquisition, supervision, and writing−review and editing.

Notes

The authors declare no competing financial interest.

■ ACKNOWLEDGMENTS

J.F. acknowledges funding from CEFT under FCT/MCTES (PIDDAC) through a postdoctoral scholarship. This work was financially supported by HealthyWaters (NORTE-01-0145-FEDER-000069), supported by Norte Portugal Regional Operational Programme (NORTE 2020), under the PORTUGAL 2020 Partnership Agreement, through the European Regional Development Fund (ERDF) and LA/P/0045/2020 (ALiCE), UIDB/00532/2020, and UIDP/00532/2020 (CEFT), funded by national funds through FCT/MCTES (PIDDAC). We also thank Daniela Silva from CEMUP (Centro de Materiais da Universidade do Porto)—Laboratório de Microscopia Eletrónica de Varrimento for performing the SEM and EDS experiments.

■ REFERENCES

(1) Galkin, O.; Vekilov, P. G. Direct Determination of the Nucleation Rates of Protein Crystals. *J. Phys. Chem. B* **1999**, *103*, 10965−10971.

(2) Ulrich, J., Stelzer, T.. *Crystallization*. 4th Ed. Wiley; Oxford, United Kingdom: Butterworth Heinemann; 2011; pp 1, 63,

(3) Manuel García-Ruiz, J. Nucleation of protein crystals. *J. Struct Biol.* **2003**, *142*, 22−31.

(4) Sleutel, M.; van Driessche, A. E. S. Nucleation of protein crystals − a nanoscopic perspective. *Nanoscale* **2018**, *10*, 12256−12267.

(5) Sleutel, M.; van Driessche, A. E. S. Role of clusters nonclassical nucleation and growth of protein crystals. *Proc. Natl. Acad. Sci. U.S.A.* **2014**, *111*, 546−553.

(6) Vekilov, P. G. Dense liquid precursor for the nucleation of ordered solid phases from solution. *Cryst. Growth Des.* **2004**, *4*, 671−685.

(7) Nicolis, G.; Maes, D. *Kinetics and thermodynamics of multistep nucleation and self-assembly in nanoscale materials*; Wiley, 2012.

(8) Kaissaratos, M.; Filobelo, L.; Vekilov, P. G. Two-Step Crystal Nucleation Is Selected because of a Lower Surface Free Energy Barrier. *Cryst. Growth Des.* **2021**, *21*, 5394−5402.

(9) Galkin, O.; Vekilov, P. G. Are nucleation kinetics of protein crystals similar to those of liquid droplets? *J. Am. Chem. Soc.* **2000**, *122*, 156−163.

(10) Ferreira, C.; Barbosa, S.; Taboada, P.; Rocha, F. A.; Damas, A. M.; Martins, P. M. The nucleation of protein crystals as a race against time with on- and off-pathways. *J. Appl. Crystallogr.* **2017**, *50*, 1056−1065.

(11) Amin, S.; Barnett, G. V.; Pathak, J. A.; Roberts, C. J.; Sarangapani, P. S. Protein aggregation, particle formation, characterization & rheology. *Curr. Opin. Colloid Interface Sci.* **2014**, *19*, 438−449.

(12) Krajina, B. A.; Tropini, C.; Zhu, A.; Digiacomo, P.; Sonnenburg, J. L.; Heilshorn, S. C.; Spakowitz, A. J. Dynamic Light Scattering Microrheology Reveals Multiscale Viscoelasticity of Polymer Gels and Precious Biological Materials. *ACS Cent. Sci.* **2017**, *3*, 1294−1303.

(13) Raynal, B.; Lenormand, P.; Baron, B.; Hoos, S.; England, P. Quality assessment and optimization of purified protein samples: Why and how? *Microb. Cell Fact.* **2014**, *13*, 180.

(14) Nobbmann, U.; Connah, M.; Fish, B.; Varley, P.; Gee, C.; Mulot, S.; Chen, J.; Zhou, L.; Lu, Y.; Sheng, F.; et al. Dynamic light scattering as a relative tool for assessing the molecular integrity and stability of monoclonal antibodies. *Biotechnol. Genet. Eng. Rev.* **2007**, *24*, 117−128.

(15) Pocker, Y.; Biswas, S. B. Conformational dynamics of insulin in solution. Circular dichroic studies. *Biochemistry* **1980**, *19*, 5043−5049.

(16) Bernson, D.; Mecinovic, A.; Abed, M. T.; Limé, F.; Jageland, P.; Palmlöf, M.; Esbjörner, E. K. Amyloid formation of bovine insulin is retarded in moderately acidic pH and by addition of short-chain alcohols. *Eur. Biophys. J.* **2020**, *49*, 145−153.

(17) Ahmad, A.; Uversky, V. N.; Hong, D.; Fink, A. L. Early Events in the Fibrillation of Monomeric Insulin. *J. Biol. Chem.* **2005**, *280*, 42669−42675.

(18) Fili, S.; Valmas, A.; Norrman, M.; Schluckebier, G.; Beckers, D.; Degen, T.; Wright, J.; Fitch, A.; Gozzo, F.; Giannopoulou, A. E.; et al. Human insulin polymorphism upon ligand binding and pH variation: The case of 4-ethylresorcinol. *IUCrJ* **2015**, *2*, 534−544.

(19) Uversky, V. N.; Garriques, L. N.; Millett, I. S.; Frokjaer, S.; Brange, J.; Doniach, S.; Fink, A. L. Prediction of the association state of insulin using spectral parameters. *J. Pharm. Sci.* **2003**, *92*, 847−858.

(20) Bohidar, H. B. Light scattering and viscosity study of heat aggregation of insulin. *Biopolymers* **1998**, *45*, 1−8.

(21) Li, Y.; Lubchenko, V.; Vekilov, P. G. The use of dynamic light scattering and Brownian microscopy to characterize protein aggregation. *Rev. Sci. Instrum.* **2011**, *82*, 1−9.

(22) Amin, S.; Rega, C. A.; Jankevics, H. Detection of viscoelasticity in aggregating dilute protein solutions through dynamic light scattering-based optical microrheology. *Rheol. Acta* **2012**, *51*, 329−342.

(23) Pathak, J. A.; Sologuren, R. R.; Narwal, R. Do clustering monoclonal antibody solutions really have a concentration dependence of viscosity? *Biophys. J.* **2013**, *104*, 913−923.

(24) Nicoud, L.; Lattuada, M.; Yates, A.; Morbidelli, M. Impact of aggregate formation on the viscosity of protein solutions. *Soft Matter* **2015**, *11*, 5513−5522.

(25) Dharmaraj, V. L.; Godfrin, P. D.; Liu, Y.; Hudson, S. D. Rheology of clustering protein solutions. *Biomicrofluidics* **2016**, *10*, 1−11.

(26) Gonçalves, A. D.; Alexander, C.; Roberts, C. J.; Spain, S. G.; Uddin, S.; Allen, S. The effect of protein concentration on the viscosity of a recombinant albumin solution formulation. *RSC Adv.* **2016**, *6*, 15143−15154.

(27) Karthika, S.; Radhakrishnan, T. K.; Kalaichelvi, P. A Review of Classical and Nonclassical Nucleation Theories. *Cryst. Growth Des.* **2016**, *16*, 6663−6681.
(28) Gebauer, D.; Raiteri, P.; Gale, J. D.; Cölfen, H. On classical and non-classical views on nucleation. *Am. J. Sci.* **2018**, *318*, 969−988.
(29) Jin, B.; Liu, Z.; Tang, R. Recent experimental explorations of non-classical nucleation. *CrystEngComm* **2020**, *22*, 4057−4073.
(30) Zhang, F.; Gavira, J. A.; Lee, G. W.; Zahn, D. Nonclassical nucleation − Role of metastable intermediate phase in crystal nucleation: An editorial prefix. *Crystals* **2021**, *11*, 174.
(31) Warzecha, M.; Florence, A. J.; Vekilov, P. G. The ambiguous functions of the precursors that enable nonclassical modes of olanzapine nucleation and growth. *Crystals* **2021**, *11*, 738.
(32) Ferreira, J.; Carneiro, J.; De Campos, J. M. Shear-Induced Crystallization and Rheological Analysis of a Therapeutic Protein. *Cryst. Growth Des.* **2022**, *22*, 6440−6455.
(33) Ferreira, J.; Sárkány, Z.; Castro, F.; Rocha, F.; Kuhn, S. Insulin crystallization: The route from hanging-drop vapour diffusion to controlled crystallization in droplet microfluidics. *J. Cryst. Growth* **2022**, *582*, 126516.
(34) Chen, F.; Du, G.; Yin, D.; Yin, R.; Zhang, H.; Zhang, W.; Yang, S. M. Crystallization of bovine insulin on a flow-free droplet-based platform. *AIP Conf. Proc.* **2017**, *1820*, 1−4.
(35) Hodzhaoglu, F. V.; Conejero-Muriel, M.; Dimitrov, I. L.; Gavira, J. A. Optimization of the classical method for nucleation and growth of rhombohedral insulin crystals by pH titration and screening. *Bulg. Chem. Commun.* **2016**, *48*, 29−37.
(36) Oza, A. U.; Venerus, D. C. The dynamics of parallel-plate and cone-plate flows. *Phys. Fluids* **2021**, *33*, 1−13.
(37) Leica Microsystems. *Microscope Software*, 2022. https://www.leica-microsystems.com/products/microscope-software/p/leica-application-suite/ (accessed Jan 1, 2023).
(38) Stetefeld, J.; McKenna, S. A.; Patel, T. R. Dynamic light scattering: a practical guide and applications in biomedical sciences. *Biophys Rev.* **2016**, *8*, 409−427.
(39) Monkos, K. Concentration and temperature dependence of viscosity in lysozyme aqueous solutions. *Biochim. Biophys. Acta* **1997**, *1339*, 304−310.
(40) Monkos, K. Viscosity analysis of the temperature dependence of the solution conformation of ovalbumin. *Biophys. Chem.* **2000**, *85*, 7−16.
(41) Peleg, M. Temperature−viscosity models reassessed. *Crit. Rev. Food Sci. Nutr.* **2018**, *58*, 2663−2672.
(42) Castellanos, M. M.; Pathak, J. A.; Leach, W.; Bishop, S. M.; Colby, R. H. Explaining the non-Newtonian character of aggregating monoclonal antibody solutions using small-angle neutron scattering. *Biophys. J.* **2014**, *107*, 469−476.
(43) Amin, S.; Barnett, G. V.; Pathak, J. A.; Roberts, C. J.; Sarangapani, P. S. Protein aggregation, particle formation, characterization & rheology. *Curr. Opin. Colloid Interface Sci.* **2014**, *19*, 438−449.
(44) Kadima, W.; McPherson, A.; Dunn, M. F.; Jurnak, F. Precrystallization aggregation of insulin by dynamic light scattering and comparison with canavalin. *J. Cryst. Growth* **1991**, *110*, 188−194.
(45) Link, F. J.; Heng, J. Y. Y. Unraveling the Impact of pH on the Crystallization of Pharmaceutical Proteins: A Case Study of Human Insulin. *Cryst. Growth Des.* **2022**, *22*, 3024−3033.
(46) Jensen, S. S.; Jensen, H.; Cornett, C.; Møller, E. H.; Østergaard, J. Insulin diffusion and self-association characterized by real-time UV imaging and Taylor dispersion analysis. *J. Pharm. Biomed. Anal.* **2014**, *92*, 203−210.
(47) Yousefi, R.; Taheri, B.; Alavi, P.; Shahsavani, M. B.; Asadi, Z.; Ghahramani, M.; Niazi, A.; Alavianmehr, M. M.; Moosavi-Movahedi, A. A. Aspirin-mediated acetylation induces structural alteration and aggregation of bovine pancreatic insulin. *J. Biomol. Struct. Dyn.* **2016**, *34*, 362−375.
(48) Kelly, S.; Price, N. The Use of Circular Dichroism in the Investigation of Protein Structure and Function. *Curr. Protein Pept. Sci.* **2000**, *1*, 349−384.
(49) Bouchard, M.; Zurdo, J.; Nettleton, E. J.; Dobson, C. M.; Robinson, C. V. Formation of insulin amyloid fibrils followed by FTIR simultaneously with CD and electron microscopy. *Protein Sci.* **2000**, *9*, 1960−1967.
(50) Nielsen, L.; Khurana, R.; Coats, A.; Frokjaer, S.; Brange, J.; Vyas, S.; Uversky, V. N.; Fink, A. L. Effect of environmental factors on the kinetics of insulin fibril formation: Elucidation of the molecular mechanism. *Biochemistry* **2001**, *40*, 6036−6046.
(51) Wei, G.; Su, Z.; Reynolds, N. P.; Arosio, P.; Hamley, I. W.; Gazit, E.; Mezzenga, R. Self-assembling peptide and protein amyloids: From structure to tailored function in nanotechnology. *Chem. Soc. Rev.* **2017**, *46*, 4661−4708.
(52) Kadima, W.; Øgendal, L.; Bauer, R.; Kaarsholm, N.; Brodersen, K.; Hansen, J. F.; Porting, P. The influence of ionic strength and pH on the aggregation properties of zinc-free insulin studied by static and dynamic laser light scattering. *Biopolymers* **1993**, *33*, 1643−1657.
(53) Hvidt, S. Insulin association in neutral solutions studied by light scattering. *Biophys. Chem.* **1991**, *39*, 205−213.
(54) Smith, M. I.; Foderà, V.; Sharp, J. S.; Roberts, C. J.; Donald, A. M. Factors affecting the formation of insulin amyloid spherulites. *Colloids Surf., B* **2012**, *89*, 216−222.
(55) Dharmaraj, V. L.; Godfrin, P. D.; Liu, Y.; Hudson, S. D. Rheology of clustering protein solutions. *Biomicrofluidics* **2016**, *10*, 1−11.
(56) Pathak, J. A.; Sologuren, R. R.; Narwal, R. Do clustering monoclonal antibody solutions really have a concentration dependence of viscosity? *Biophys. J.* **2013**, *104*, 913−923.
(57) Amin, S.; Rega, C. A.; Jankevics, H. Detection of viscoelasticity in aggregating dilute protein solutions through dynamic light scattering-based optical microrheology. *Rheol. Acta* **2012**, *51*, 329−342.
(58) Ducruix, A.; Giegé, R. *Crystallization of Nucleic Acids and Proteins: A Practical Approach*. 2nd ed.; Oxford University Press, 1999.
(59) McPherson, A.; Gavira, J. A. Introduction to protein crystallization. *Acta Crystallogr., Sect. F: Struct. Biol. Commun.* **2014**, *70*, 2−20.

https://doi.org/10.1021/acsomega.3c10052
ACS Omega 2024, 9, 23364−23376